High Power Laser Science and Engineering, (2024), Vol. 12, e87, 10 pages.
doi:10.1017/hpl.2024.71

RESEARCH ARTICLE

A 606 W burst-mode picosecond Yb-doped all-fiber laser with an intra-burst repetition rate of 469 MHz

Xinyao Li[1,2,3,4], Haijuan Yu[1,2,3,4], Shuzhen Zou[1,4], Chaojian He[1,4], Chaoyu Ning[1,5], Wenjuan Wu[1,2,3,4], Xuechun Chen[1,5], and Xuechun Lin[1,2,3,4]

[1] *Laboratory of All-Solid-State Light Sources, Institute of Semiconductors, Chinese Academy of Sciences, Beijing, China*

[2] *College of Materials Science and Opto-Electronic Technology, University of Chinese Academy of Sciences, Beijing, China*

[3] *Center of Materials Science and Optoelectronics Engineering, University of Chinese Academy of Sciences, Beijing, China*

[4] *Beijing Engineering Technology Research Center of All-Solid-State Lasers Advanced Manufacturing, Beijing, China*

[5] *Southwest Institute of Technical Physics, Chengdu, China*

(Received 26 July 2024; revised 10 September 2024; accepted 12 October 2024)

Abstract

This paper introduces a novel fiber-based picosecond burst-mode laser system capable of operating at high power and high repetition rates. A pulse-circulating fiber ring was developed as a burst generator, achieving an intra-burst repetition rate of 469 MHz without the need for a high-repetition-rate seed source. This design also allows for flexible adjustment of the number of sub-pulses, burst repetition rate and burst shape. In addition, a master oscillator power amplifier was employed to analyze the amplification characteristics of bursts. The system demonstrated a maximum average power of 606 W, with a measured sub-pulse duration of 62 ps and the highest sub-pulse peak power of 980 kW. To the best of our knowledge, this marks the highest average power obtained in burst-mode ultrafast lasers. Such a laser system holds potential for applications in precision manufacturing, high-speed imaging, high-precision ranging and other diverse domains.

Keywords: burst-mode laser; high power; high repetition rate; picosecond fiber laser

1. Introduction

Ultra-short pulse lasers represent a significant optical technology widely applied in optical communication, biomedicine, material processing and scientific research. In precision manufacturing, burst-mode lasers, particularly those with GHz intra-burst repetition rates, promise enhanced efficiency and quality through ablation cooling[1]. Numerous studies have demonstrated the superior materials processing and manufacturing performances of GHz burst-mode[2–10] or biburst-mode lasers[11–16]. Due to the compact structure, high stability, robustness and cost-effectiveness of fiber laser systems, pursuing high-power, high-repetition-rate burst-mode all-fiber lasers has become a crucial research topic in ultrafast optics.

Time domain modulation is commonly utilized in the production of burst-mode lasers, but it presents certain constraints. Direct modulation of rectangular nanosecond pulses using an electro-optic modulator (EOM) has enabled the realization of burst-mode lasers with sub-pulse repetition rates ranging from 0.5 to 10 GHz[17]. However, this approach requires an exceptionally fast EOM and a robust power supply. In addition, the pulse duration is limited by the rise and fall times of the EOM. The use of an acoustic-optic modulator (AOM) to select specific pulses for burst formation preserves the inherent characteristics of ultrafast pulses and provides a wide range of burst parameter management[18–20]. Even so, it strongly demands a high-repetition-rate pulse seed source to operate in GHz burst mode. The repetition rate multiplication method based on cascaded fiber couplers and delay lines can increase the repetition rate from MHz to several GHz, but it faces difficulties in maintaining consistent pulse energies and accurate pulse spacing[5,21–24]. Harmonic mode-locking technology, which can achieve pulse repetition rates in the GHz range, suffers from issues related to stability and timing jitter[25–27]. Recently, fundamentally mode-locked fiber lasers with ultra-short resonant cavities of centimeter or sub-centimeter scale have been reported to operate at repetition rates surpassing 10 GHz[28–31]. However, the feasibility of these systems heavily relies on the advancements in highly doped active fibers and the seamless integration of intracavity components[32–34]. Therefore, developing a fiber laser that supports GHz burst-mode remains a pressing challenge.

Correspondence to: X. Lin and H. Yu, Laboratory of All-Solid-State Light Sources, Institute of Semiconductors, Chinese Academy of Sciences, Beijing 100083, China. Emails: xclin@semi.ac.cn (X. Lin); hjyu@semi.ac.cn (H. Yu)

Moreover, the abundant nonlinear effects inherent in fibers, such as self-phase modulation (SPM) and stimulated Raman scattering (SRS), bring significant obstacles to attaining high average and peak powers in all-fiber configurations. Picosecond pulse lasers have achieved kW-level output power due to the flourishing development of large-mode-area fiber fabrication technology[35,36]. Nevertheless, picosecond burst-mode lasers with increased single-pulse energy and peak power encounter more difficulties in power raising. For example, in a study by Yu *et al.* in 2015[37], picosecond burst-mode laser output reached an average power of 85 W using a *Q*-switched mode-locked oscillator and a master oscillator power amplifier (MOPA) amplification system. In 2018, the average power was increased to 166 W, with a burst energy of 8.3 mJ[38]. In 2022, Liu *et al.*[39] demonstrated GHz bursts with a tunable intra-burst repetition rate ranging from 0.8 to 1.5 GHz, delivering a maximum average power of 304 W. In 2023, they used extra-large-mode-area (XLMA) fibers to attain a burst energy of 13.3 mJ, with a sub-pulse duration of 48 ps[17]. Despite these advances, the output powers still cannot match the levels achievable with picosecond pulsed lasers. Consequently, overcoming the difficulties posed by nonlinear effects to realize high-repetition-rate, high-power picosecond burst-mode all-fiber lasers is crucial.

This work presents an innovative all-fiber system that employs a gain fiber ring to circulate multiple pulses and produce high-repetition-rate burst-mode lasers. The intra-burst repetition rate reached 469 MHz, independent of the repetition rate of the seed pulse. The burst repetition rate ranged from 103 kHz to 2.06 MHz, the number of sub-pulses varied from two to seven and various burst shapes were possible, offering considerable flexibility. A multi-stage fiber amplifier was developed to investigate the amplification properties of the bursts under various parameters. Experimental results indicated that the primary limitation on increasing burst power was the SRS effect induced by the high peak power of the sub-pulses. Ultimately, a remarkable average power of 606 W was accomplished, which is the highest average power reported in ultrafast burst-mode lasers. The sub-pulse duration was measured at 62 ps, with the highest sub-pulse peak power reaching 980 kW. This laser system extends the potential applications of high-power, high-repetition-rate burst-mode lasers beyond laser processing to diverse fields including astronomical observation, radar and optical communication, highlighting its broad practical significance.

2. High-repetition-rate burst generator

2.1. Structure and principle of high-repetition-rate burst generator

The burst generator scheme shown in Figure 1(a) mainly consists of a gain fiber ring, which comprises a 2 × 2 fiber coupler, an isolator, an amplifier, a segment of passive fiber and AOM1 to support multi-pulse circulation and create bursts. AOM2, located outside the ring, acts as a pulse picker to select bursts with a specific number of pulses. The amplifier in the fiber ring utilizes a 3 m Yb^{3+}-doped fiber (Nufern LMA-YDF-10/125-9M), pumped by a 5 W 976 nm multi-mode laser diode (LD) through a (2 + 1) ×1 signal-pump combiner. The two AOMs, each with a rise time of 10 ns, are synchronized using an arbitrary waveform generator (AWG).

The pulse cycling process starts with a pulse train entering the coupler through the in1 port, featuring a repetition rate of f_0 and a period of T_0. This train splits into two sub-pulses: one is output from the out1 port as the output sub-pulse, while the other enters the fiber ring via the out2 port as the cyclic sub-pulse. Within the fiber ring, the cyclic sub-pulse undergoes amplification and selection before re-entering the coupler through the in2 port. When it is recombined with a subsequent output sub-pulse of the initial pulse train, a double-pulse burst is formed with a time interval of $T_2 = T_1 - T_0$. At this point, one pulse cycle is completed. Here, T_1 represents the propagation time of the pulse in the fiber ring. After N cycles, a burst containing up to $N+1$ sub-pulses will be obtained, as depicted in Figure 1(b). It is worth noting that the time interval of the sub-pulses is entirely determined by T_1, which depends on the length of the fiber ring rather than the initial pulse. Therefore, high-repetition-rate bursts can be easily obtained by properly controlling the fiber ring length. Accurate regulation of both the maximum number of sub-pulses per burst and the burst repetition rate is accomplished through fine-tuning the opening time (T_{AOM1}) and switching frequency (f_{AOM1}) of AOM1, as illustrated in Figure 1(b). Furthermore, by varying the opening time (T_{AOM2}) of AOM2, two distinct burst modes can be activated: the variational biburst mode (when $T_0 < T_{AOM2} < T_{AOM1}$), where multiple bursts with an increasing number of sub-pulses, separated by a time interval T_0, are combined into larger bursts and repeated at f_{AOM1}, as shown in Figure 1(c); or the identical burst mode (when $T_{AOM2} \leq T_0$), where several bursts with the same number of sub-pulses are repeated at a frequency of f_{AOM1}, as shown in Figure 1(d). To maintain burst stability, ensure that the switching frequency of AOM2 aligns with that of AOM1. Adjusting the time delay T_d between AOM2 and AOM1 can change the number of sub-pulses in each burst. The fiber amplifier compensates for losses within the ring to sustain efficient pulse circulation.

2.2. Output characteristics of high-repetition-rate bursts

A home-built semiconductor saturable absorber mirror (SESAM) mode-locked fiber laser oscillator, as depicted in Figure 1(a), produces the initial pulse train with a center wavelength of 1064 nm and a time interval of 48.5 ns. The corresponding oscilloscope trace is presented in Figure 1(b). The radio frequency (RF) spectrum is acquired

https://doi.org/10.1017/hpl.2024.71 Published online by Cambridge University Press

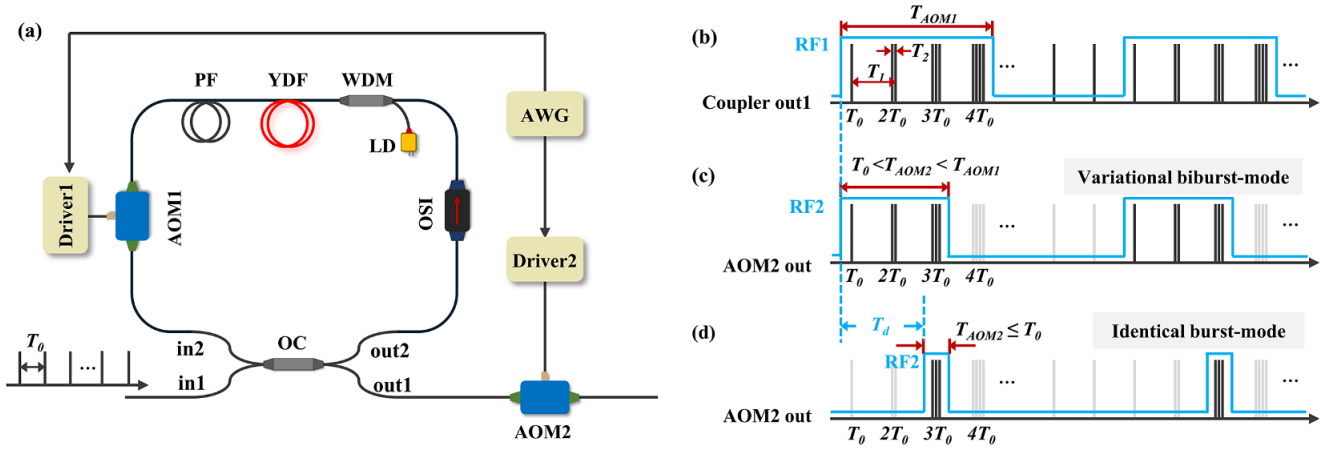

Figure 1. (a) Schematic diagram of the high-repetition-rate burst generator. OC, optical fiber coupler; ISO, fiber isolator; LD, laser diode; WDM, wavelength division multiplexer; YDF, Yb^{3+}-doped fiber; PF, passive fiber; AOM, acoustic-optic modulator; AWG, arbitrary waveform generator. (b) Burst-mode and single-pulse-mode laser output from the out1 port of the coupler. (c) Variational biburst-mode laser output from AOM2. (d) Identical burst-mode laser output from AOM2. RF, radio frequency signal.

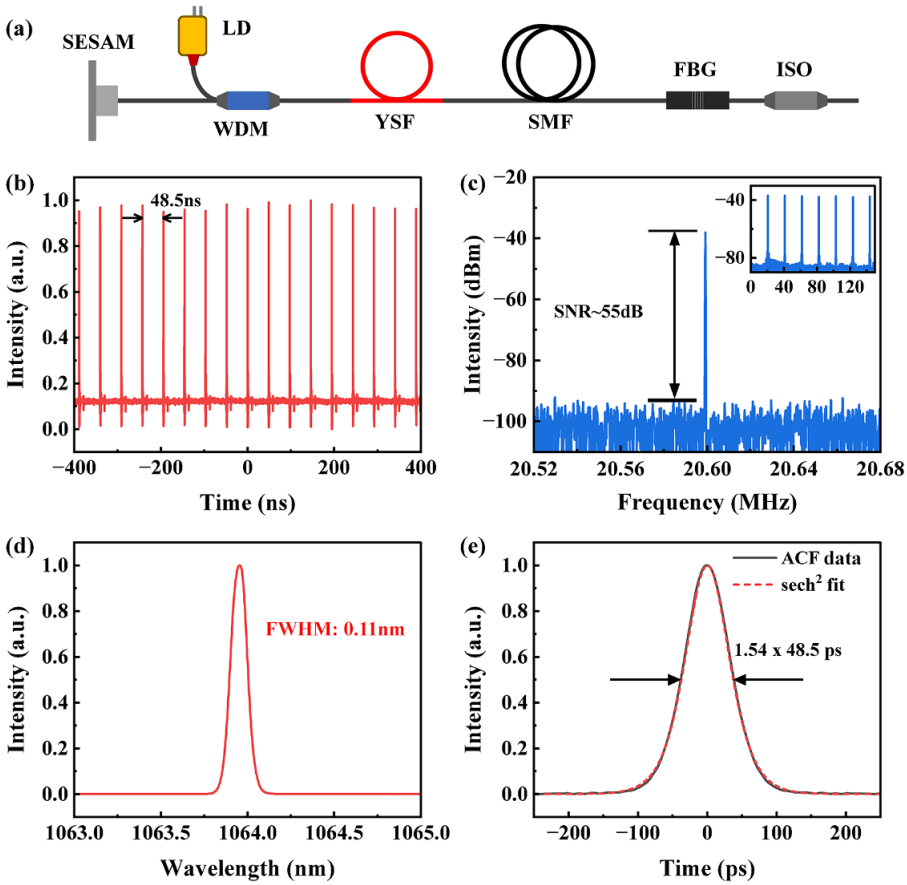

Figure 2. (a) Scheme of the mode-locked fiber laser oscillator. YSF, Yb^{3+}-doped single mode fiber; SMF, passive single mode fiber; FBG, fiber Bragg grating. (b) Typical pulse train of the oscillator recorded using a digital oscilloscope (Keysight DSOS404A) and a photodetector (Thorlabs DET08CL/M). (c) RF spectrum of the mode-locked pulse measured by the oscilloscope mentioned above. Inset: the broad-span RF output spectrum. (d) Optical spectrum of the mode-locked pulse measured with an optical spectrum analyzer (Yokogawa AQ6370D). (e) Autocorrelation trace of the mode-locked pulse obtained using an autocorrelator (APE SM2000).

at a resolution bandwidth (RBW) of 100 Hz, as shown in Figure 2(c), revealing a fundamental frequency of 20.6 MHz and a signal-to-noise ratio (SNR) of 55 dB. Over a wider frequency span, no sidelobes or satellite peaks are detected, confirming a stable operation. After one stage amplification, the output power reaches 50 mW, with a –3 dB spectral bandwidth of 0.11 nm and a pulse duration of 48.5 ps, as depicted in Figures 2(d) and 2(e).

https://doi.org/10.1017/hpl.2024.71 Published online by Cambridge University Press

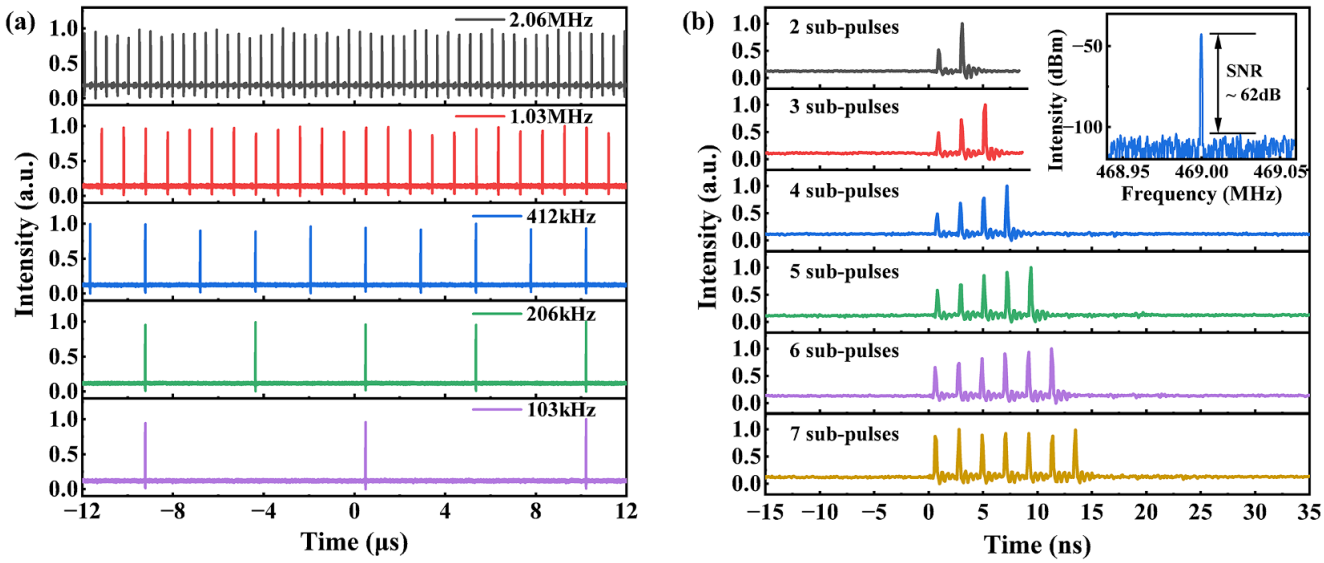

Figure 3. (a) Identical burst modes with burst repetition rates of 2.06 MHz, 1.03 MHz, 412 kHz, 206 kHz and 103 kHz, respectively. (b) Single burst with two to seven sub-pulses. Inset: RF spectrum of the bursts.

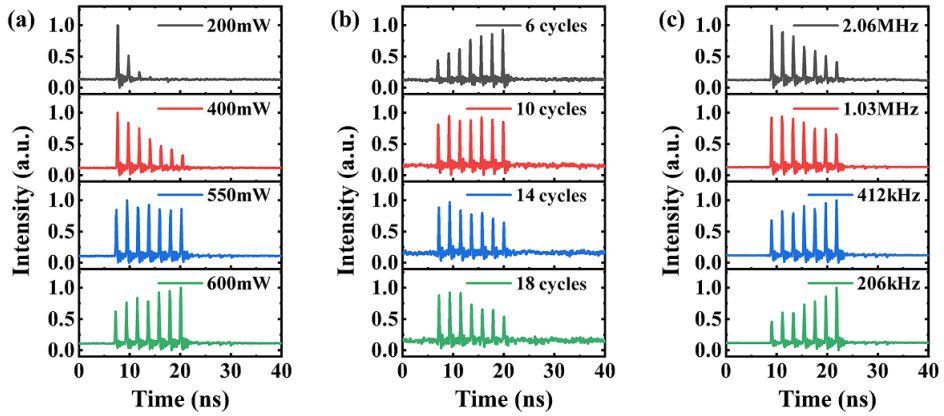

Figure 4. Burst envelope shapes in different cases. (a) AOM1 switch frequency set to 1.03 MHz with an open time of 350 ns, and amplifier pump powers of 200, 400, 550 and 600 mW. (b) Pump power of 500 mW with AOM1 switch frequency at 412 kHz, and pulse cycle counts of 6, 10, 14, and 18. (c) Pump power of 500 mW with AOM1 open time of 350 ns, and switch frequencies of 2.06 MHz, 1.03 MHz, 412 kHz and 206 kHz.

The total length of the fiber ring is precisely controlled at 10.13 m, yielding a sub-pulse time interval of approximately 2.13 ns. The inset in Figure 3(b) shows the RF spectrum of the burst-mode laser recorded between 468.94 and 469.06 MHz at a 100 Hz RBW. The result shows a frequency of 469 MHz with a 62 dB SNR, corresponding to the sub-pulse interval. The repetition rate of the generated bursts can be flexibly adjusted between 2.06 MHz and 103 kHz using the AWG, as illustrated in Figure 3(a). The maximum number of sub-pulses, n, primarily depends on the ratio of the pulse interval T_0 of the initial pulse train to the cyclic sub-pulse interval T_2, that is, $n \leq (T_0/T_2) + 1$. For the initial pulse interval $T_0 = 48.5$ ns and the sub-pulse interval $T_2 = 2.13$ ns in our system, the generated burst contains a maximum of 23 sub-pulses. In theory, bursts containing hundreds or even thousands of sub-pulses could be achieved by increasing T_0 and reducing T_2. In this experiment, we primarily selected an identical burst mode as the input signal for the subsequent amplifier to study the burst amplification performance under different parameters. However, currently, we can only achieve a time delay T_d of approximately 250 ns through a dual-channel AWG. As a result, the number of sub-pulses in the burst output from AOM2 can be adjusted between two and seven, as shown in Figure 3(b). If a longer T_d can be realized through improved electrical signal control, this system could potentially generate bursts with an adjustable number of sub-pulses ranging from 2 to 23 in the future.

In addition, this system supports the design of the burst temporal envelope shape, which is a critical feature in burst-mode lasers[40–43]. Firstly, by changing the pump power of the amplifier to exactly manipulate the intensity of each sub-pulse, the burst shape can transform from ‘decaying amplitude’ to ‘equal amplitude’ to ‘rising amplitude’, as

https://doi.org/10.1017/hpl.2024.71 Published online by Cambridge University Press

depicted in Figure 4(a). Secondly, the burst shape can also be altered by maintaining a constant pump power while varying the open time and switching frequency of AOM1. For example, in Figure 4(b), with the AOM1 switching frequency held at 1.03 MHz, extending the open time to increase the number of pulse cycles from 6 to 18 counts changes the burst shape from 'rising amplitude' to 'decaying amplitude'. In contrast, by fixing the open time of AOM1 at 350 ns and reducing the switching frequency from 2.06 MHz to 206 kHz, the burst shape undergoes the opposite change, as illustrated in Figure 4(c). These phenomena can be attributed to the extraction of pump energy by the circulating pulses. With constant pump power in the ring and a fixed number of sub-pulses in the burst, if the AOM switching frequency remains unchanged, a longer AOM open time allows more sub-pulses to circulate in the ring. As a result, sub-pulses at the trailing edge of the burst extract less energy and feature lower intensity than those at the leading edge, presenting a descending shape. Conversely, fixing the AOM open time while decreasing the switching frequency leads to more energy extraction by sub-pulses at the trailing edge, resulting in higher intensity and a rising shape.

In summary, the innovative burst generator based on the gain fiber ring has the advantages of compact structure, cost-effectiveness and good robustness. It can generate a high-repetition-rate burst-mode laser without relying on excellent mode-locked pulse seed and optical modulation devices. By modifying the gain, AOM opening time and switching frequency in this system, parameters including the number of sub-pulses, burst repetition rate and burst temporal shape can be controlled simultaneously.

3. Multi-stage amplifiers of high-repetition-rate bursts

To enhance the output power of the burst-mode laser, we developed an all-fiber power amplification system comprising three pre-amplifiers and a main amplifier, as depicted in Figure 5. The first two cascaded pre-amplifiers utilize components identical to those in the amplifier of the gain fiber ring. The third pre-amplifier employs a 3 m Yb^{3+}-doped fiber with a large mode area (Nufern LMA-YDF-30/250-HI-8), pumped by two 30 W fiber-pigtailed 976 nm LDs through a $(6 + 1) \times 1$ signal/pump combiner. The output signal is then further boosted in the main amplifier, which contains a 2 m XLMA Yb^{3+}-doped fiber with core/inner cladding diameters of 100/400 μm (core numerical aperture (NA) of 0.11, cladding absorption coefficient of approximately 6 dB/m at 915 nm). Six 976 nm multi-mode LDs, each capable of delivering up to 180 W, serve as pump sources for the active fiber via a $(6 + 1) \times 1$ signal/pump combiner. Besides, a fiber-pigtailed end cap is fused to the output end of the system to mitigate unwanted end reflections and prevent fiber facet damage. Meanwhile, an isolator with bandpass filter (IBP) and a cladding pump stripper (CPS) are applied to each amplifier stage to protect the front structure from damage and eliminate the residual pumping light in the cladding, respectively. All optical components, except for the end cap, are mounted on the water-cooled heat sinks.

Due to significant power loss from pulse selection and the device's insertion loss, the maximum average output power of the burst generator is less than 5 mW. Amplified spontaneous emission (ASE) poses a risk to the weak burst signals during power scaling, leading to a decline in the SNR and potential system instability. Hence, two cascaded 10/125 μm fiber amplifiers were implemented with careful gain management at each stage to mitigate ASE. This enabled the burst power to be increased to around 1 W under various parameters while maintaining an excellent SNR, sufficient to saturate the third pre-amplification stage.

As burst power increases, the influence of the SRS effect becomes increasingly evident in subsequent amplification stages. The spectra depicted in Figure 6(a) reveal that bursts at a repetition rate of 412 kHz, composed of three sub-pulses, exhibit an SNR of less than 20 dB relative to the first-order SRS at an average output power of 9.3 W. In Figure 6(b), the red dashed line indicates the estimated first-order SRS power ratio of bursts at varying pump powers. For bursts repeating at 2.06 MHz with three and seven sub-pulses, as well as those at 1.03 MHz with seven sub-pulses, the SRS power ratio remains below 0.1% as the pump power increases. Instead, bursts at 1.03 MHz with three sub-pulses, and at 412 kHz with three and seven sub-pulses, exhibit an exponential increase in the SRS ratio beyond a certain pump power. At 20 W pump power, bursts with 412 kHz repetition rate and three sub-pulses reach an SRS ratio of 12%, attributed to the rapid increase in peak power of the sub-pulses. The average sub-pulse peak power exceeds 70 kW, surpassing the SRS threshold for a 30 μm core diameter fiber. Bursts at 1.03 MHz with three sub-pulses and those at 412 kHz with seven sub-pulses maintain a closely aligned average sub-pulse peak power and SRS ratio due to their comparable total number of sub-pulses, as presented in Figure 6(b). This underscores the crucial impact of peak power on burst amplification. Higher burst repetition rates and increased sub-pulses numbers collaborate to decrease sub-pulse peak power, which can effectively mitigate nonlinear effects and facilitate high power output.

The SRS effect typically involves the transfer of signal energy to Raman wavelengths, leading to a decrease in signal power, which in turn lowers pump conversion efficiency and impacts system stability. To address this issue, a bandpass filter was spliced at the output of the third pre-amplifier to eliminate the SRS component, ensuring that the cleanest signal is injected into the final amplifier stage. At this point, the output powers of bursts with repetition rates of 2.06 MHz, 1.03 MHz and 412 kHz are approximately 10, 6.8 and 3.2 W,

https://doi.org/10.1017/hpl.2024.71 Published online by Cambridge University Press

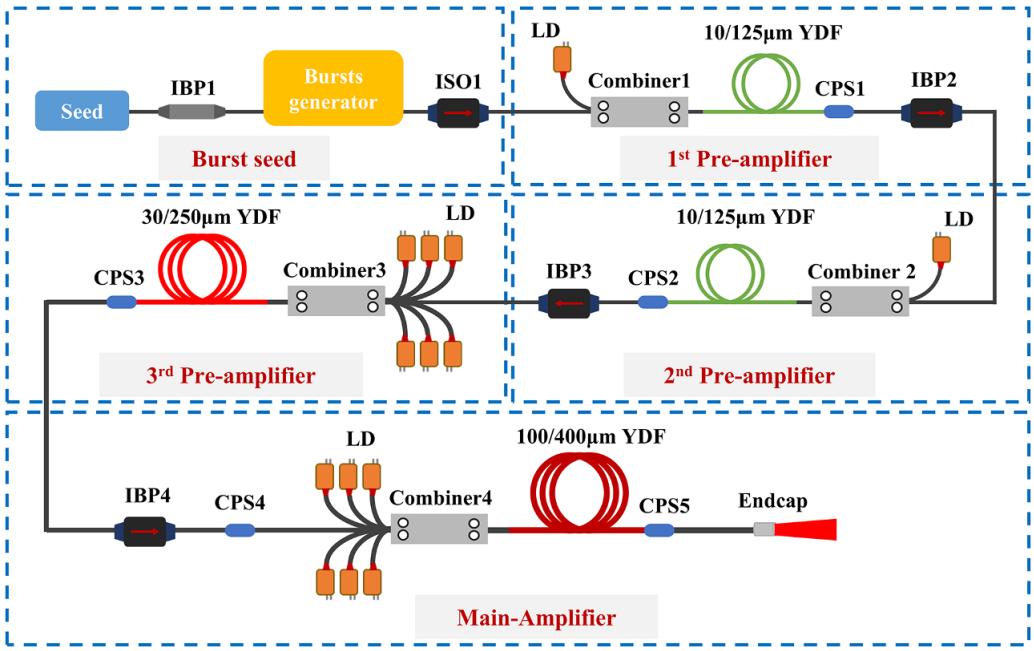

Figure 5. Experimental setup of the burst amplification system. IBP, isolator with bandpass filter; ISO, isolator; CPS, cladding pump stripper.

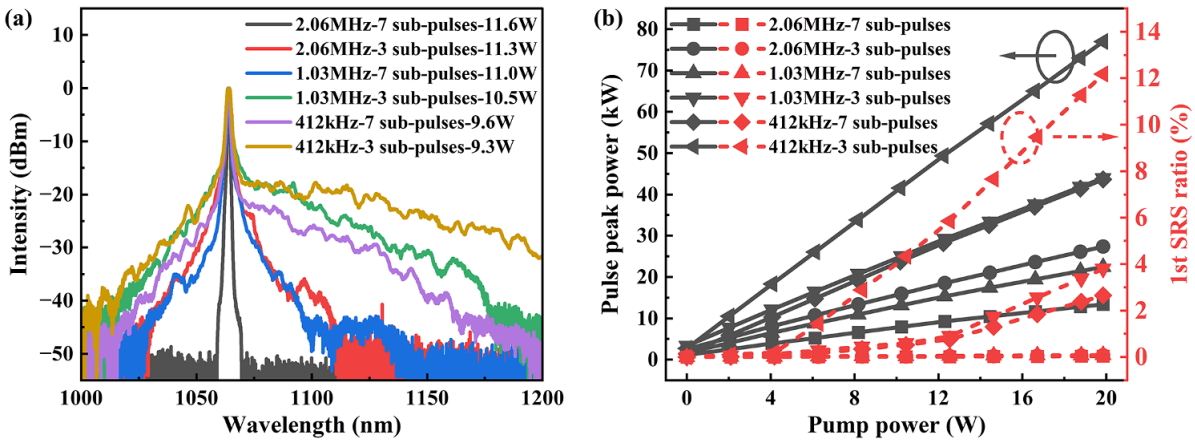

Figure 6. Output characteristics of bursts with repetition rates of 2.06 MHz, 1.03 MHz and 412 kHz, and sub-pulses number of seven and three, respectively. (a) Output spectra at an average output power of approximately 10 W. (b) Average sub-pulse peak power (black solid curve) and the first-order SRS power ratio (red dotted curve) versus pump power.

respectively. In addition, XLMA gain fiber was used in the main amplifier to increase the SRS threshold and further enhance the burst power. Despite these, the output spectrum of bursts containing seven sub-pulses at a repetition rate of 412 kHz still displays unexpected wavelength components beyond 1100 nm, as illustrated in Figure 7(c). This additional noise, amplified alongside the central wavelength signal, lowers the nonlinear threshold. Figure 8(a) demonstrates that these bursts already exhibit first-order SRS at approximately 50 W pump power. With a pump power increase to 180 W, the SRS ratio exceeds 15%, resulting in an output average power of 132 W, corresponding to an average sub-pulse peak power of 670 kW.

In contrast, bursts at repetition rates of 1.03 and 2.06 MHz show relatively clearer spectra, as depicted in Figures 7(a) and 7(b), indicating a higher SRS threshold. However, at around 15% SRS power ratio, their average sub-pulse peak powers match that of the 412 kHz case. The higher repetition rates lead to more sub-pulses per unit time, thereby reaching higher average power outputs. Specifically, bursts at 1.03 and 2.06 MHz, each containing seven sub-pulses, attain maximum average power outputs of 319 and 606 W, respectively. In cases of fewer sub-pulses, the average sub-pulse peak power increases more rapidly with pump power, causing severe nonlinear effects and reduced output power. At 2.06 MHz, bursts with two to six sub-pulses in the main amplifier realize maximum average output powers of 116, 213, 362, 460 and 558 W, respectively. The slope efficiency of these bursts is up to 83%, as illustrated in Figure 8(b). Although the growth rate of the net signal power decreases

https://doi.org/10.1017/hpl.2024.71 Published online by Cambridge University Press

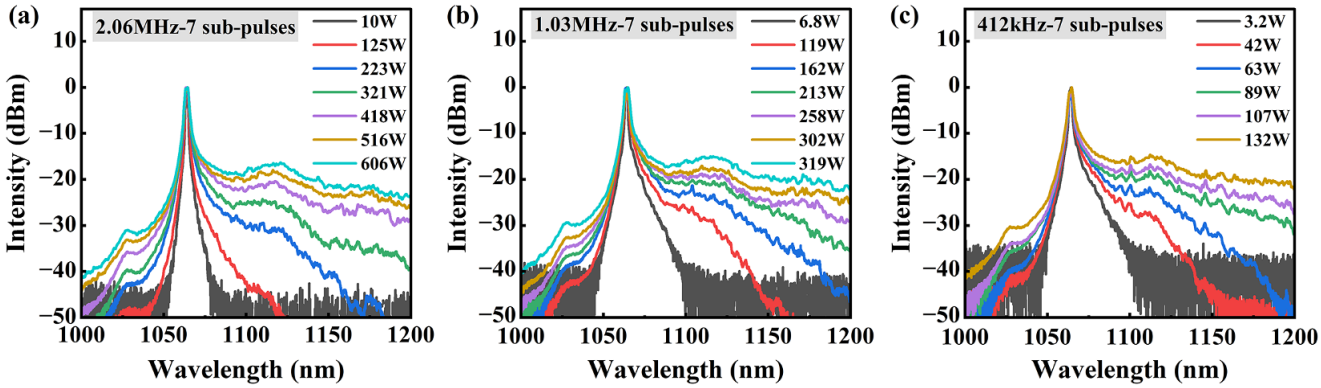

Figure 7. Output spectra of bursts with seven sub-pulses and burst repetition rates of (a) 2.06 MHz, (b) 1.03 MHz and (c) 412 kHz at different output powers.

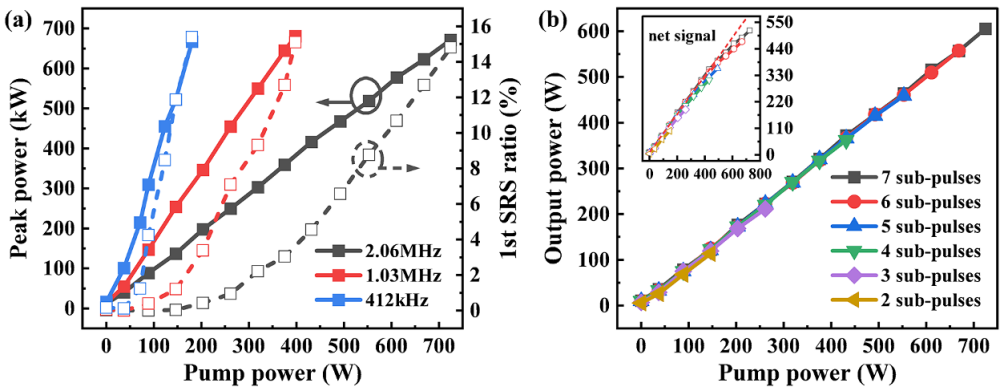

Figure 8. (a) Average sub-pulse peak power (solid line) and first-order SRS power ratio (dotted line) versus pump power for bursts containing seven sub-pulses at repetition rates of 2.06 MHz, 1.03 MHz and 412 kHz. (b) Output average power of bursts containing two to seven sub-pulses at a repetition rate of 2.06 MHz as a function of pump power. Inset: net signal average power of bursts containing two to seven sub-pulses at a repetition rate of 2.06 MHz as a function of pump power, where the line and symbol colors are consistent with the main figure for the same number of sub-pulses.

at higher power levels due to the onset of SRS, as shown in the inset of Figure 8(b), an output power of 520 W is still achieved. The normalized linear spectrum at the maximum power is illustrated in Figure 9(a). The region highlighted in light red represents the SRS component, which clearly constitutes a small proportion compared to the signal wavelength. Due to the SPM effect, the –3 dB spectral width bandwidth at this power level broadens to 2.61 nm. The final pulse duration of 62 ps is derived from the deconvolution of the pulse autocorrelation trace fitted with a sech^2 function, as described in Figure 9(b).

To weaken the adverse effects of gain saturation when amplifying long pulses ranging from nanoseconds to microseconds[44–46], precise control over pump power and pulse cycle counts is carried out in the burst generator. This ensures that burst seeds are acquired with a pre-compensated temporal shape. However, the saturation energy of a single pulse can reach several millijoules for an XLMA gain fiber with a core diameter of 100 μm[37,41]. This significantly exceeds the maximum burst energy of 340 μJ delivered by the main amplifier. Therefore, the temporal profiles of burst do not exhibit significant changes with increasing power, as shown in Figure 10. Analysis of burst energy and envelope characteristics allows estimation of the energy and peak power of each sub-pulse within the bursts, reaching maximum values of 61 μJ and 980 kW, respectively.

Moreover, we measured the radiation stability of the burst-mode fiber laser system, with the relative intensity noise (RIN) results presented in Figure 11(a). The RIN is mostly sustained before and after the burst generator but deteriorates after the main amplifier. As the frequency increases from 10 Hz to 1 MHz, the RIN decreases from −83 to −110 dBc/Hz, and the corresponding integrated RIN is calculated to be less than 0.35%, compared to 0.15% for the mode-locked seed. Future improvements in the noise performance of the amplification system could be achieved by stabilizing the pump source, reducing nonlinear effects and applying active stabilization techniques. The long-term stability of the final output was monitored at an output power of 606 W over 1 hour. The relative standard deviation of power fluctuation is less than 0.23%, which confirms the satisfactory stability over time.

Furthermore, the beam quality at the highest output power of 606 W is depicted in Figure 11(a), with an M^2 value of approximately 11.51 ($M^2_x = 11.58$, $M^2_y = 11.44$). Although the use of gain fiber with an extra-large-mode area in the

https://doi.org/10.1017/hpl.2024.71 Published online by Cambridge University Press

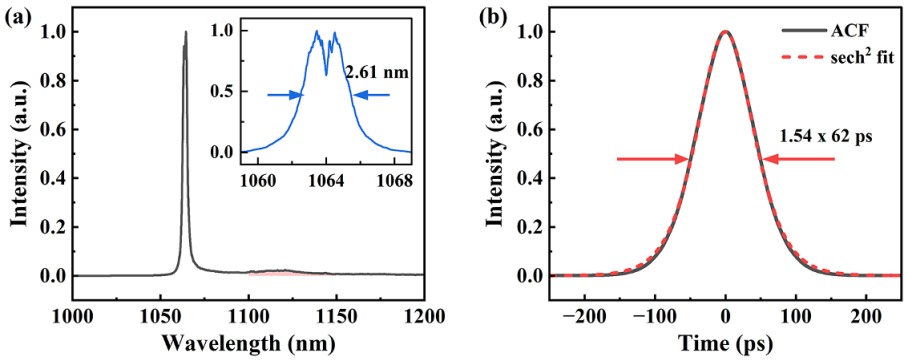

Figure 9. Characteristics of bursts at the maximum average power of 606 W. (a) Output spectrum, where the light red region represents the first-order SRS component. Inset: detailed spectrum in the range of 1059–1069 nm. (b) Autocorrelation trace.

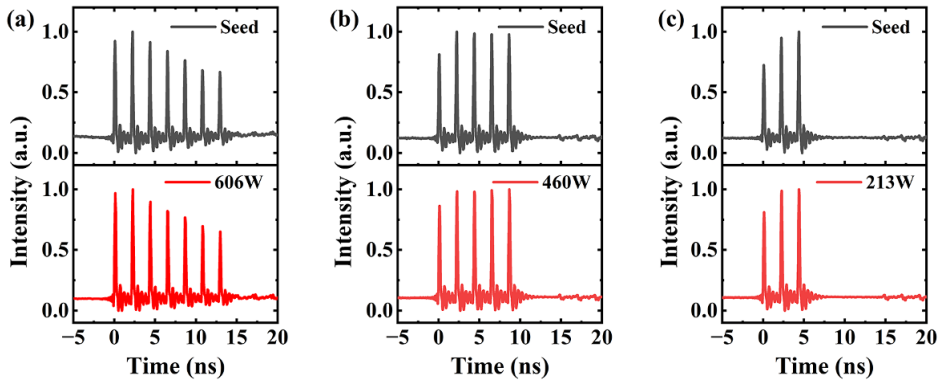

Figure 10. Envelope shapes of bursts containing (a) seven sub-pulses, (b) five sub-pulses and (c) three sub-pulses at different output powers.

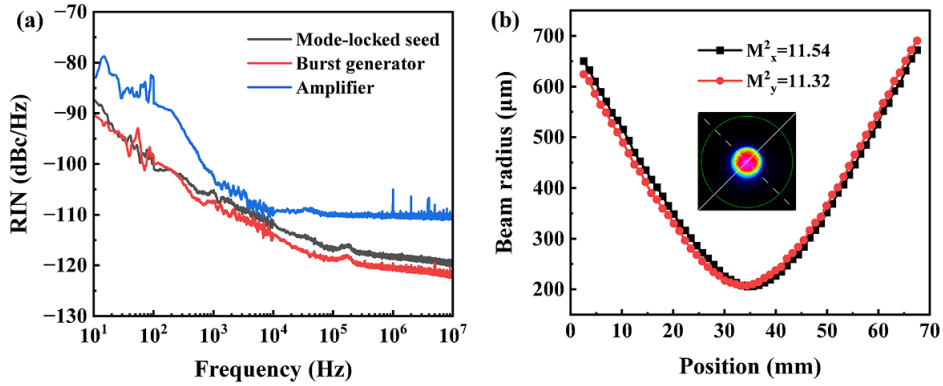

Figure 11. (a) Relative intensity noise (RIN) measured of the mode-locked seed, burst generator and main amplifier. (b) Beam profile and M^2 factor at the maximum output power of 606 W.

main amplifier can suppress the SRS effect and increase the output power, it sacrifices the single-mode characteristics of the laser, which deteriorates the beam quality and radiation brightness. In fact, many studies have proved that near-diffraction-limited lasers can be realized by employing special structure fibers such as tapered fibers, chirally coupled-core fibers and photonic crystal fibers[47–50]. At the same time, these fibers are also conducive to weakening nonlinear effects and achieving higher output powers, thereby further improving the radiation brightness of such burst-mode fiber laser systems and expanding their potential applications in the future.

4. Conclusion

We have developed a burst generator based on a gain fiber ring that converts a low-repetition-rate pulse train into high-repetition-rate bursts through a pulse-circulating mechanism. This setup does not require extremely high-performance optical modulators or seed sources, and the time interval of sub-pulses within the generated burst only depends on the length of the fiber ring. Experimentally, bursts with an intra-burst repetition rate of 469 MHz have been reliably generated. In addition, the number of sub-pulses, burst repetition rate and burst envelope shape can be modulated

https://doi.org/10.1017/hpl.2024.71 Published online by Cambridge University Press

simultaneously by adjusting parameters such as the gain, AOM opening time and switching frequency. In theory, arbitrary bursts with intra-burst repetition rates exceeding 10 GHz can be easily realized. By studying the amplification characteristics of bursts with different configurations, we found that the SRS effect mainly limits the power enhancement, which is particularly obvious in bursts with fewer total sub-pulses. Finally, the laser system achieved a maximum average power of 606 W, with the highest sub-pulse energy reaching 61 μJ and peak power of 980 kW. In the future, the spectral SNR needs to be further improved, and the number of sub-pulses with each burst and flexibility of the burst shape require optimization to enhance applicability. This high-repetition-rate, high-power ultrafast burst-mode laser is expected to satisfy various precision processing requirements and, at the same time, extend its application to other fields, such as astronomical measurements and photon microwave generation, thereby fostering innovation in these areas.

Acknowledgments

This work was financially supported by the CAS Project for Young Scientists in Basic Research (No. YSBR-065), the National Natural Science Foundation of China (Nos. 62225507, 62175230, 62175232 and 62275244) and the National Key R&D Program of China (No. 2022YFB3607800). The authors would like to sincerely thank Prof. Jing-Yuan Zhang for his valuable suggestions in writing the manuscript.

References

1. C. Kerse, H. Kalaycıoğlu, P. Elahi, B. Çetin, D. K. Kesim, Ö. Akçaalan, S. Yavaş, M. D. Aşık, B. Öktem, H. Hoogland, R. Holzwarth, and F. Ö. Ilday, Nature **537**, 84 (2016).
2. D. Metzner, P. Lickschat, and S. Weissmantel, Appl. Surf. Sci. **531**, 147270 (2020).
3. S. Butkus, V. Jukna, D. Paipulas, M. Barkauskas, and V. Sirutkaitis, Micromachines **11**, 733 (2020).
4. G. Bonamis, K. Mishchick, E. Audouard, C. Honninger, E. Mottay, J. Lopez, and I. Manek-Honninger, J. Laser Appl. **31**, 022205 (2019).
5. K. Mishchik, G. Bonamis, J. Qiao, J. Lopez, E. Audouard, E. Mottay, C. Honninger, and I. Manek-Honninger, Opt. Lett. **44**, 2193 (2019).
6. G. Bonamis, E. Audouard, C. Hönninger, J. Lopez, K. Mishchik, E. Mottay, and I. Manek-Hönninger, Opt. Express **28**, 27702 (2020).
7. M. Park, Y. R. Gu, X. L. Mao, C. P. Grigoropoulos, and V. Zorba, Sci. Adv. **9**, eadf6397 (2023).
8. S. Kawabata, S. Bai, K. Obata, G. Miyaji, and K. Sugioka, Int. J. Extreme Manuf. **5**, 015004 (2023).
9. E. Audouard and E. Mottay, Int. J. Adv. Manuf. Technol. **5**, 015003 (2023).
10. J. Lopez, S. Niane, G. Bonamis, P. Balage, E. Audouard, C. Hönninger, E. Mottay, and I. Manek-Hönninger, Opt. Express **30**, 12533 (2022).
11. K. Obata, F. Caballero-Lucas, S. Kawabata, G. Miyaji, and K. Sugioka, Int. J. Adv. Manuf. Technol. **5**, 025002 (2023).
12. F. Caballero-Lucas, K. Obata, and K. Sugioka, Int. J. Extreme Manuf. **4**, 015103 (2022).
13. A. Žemaitis, M. Gaidys, P. Gečys, M. Barkauskas, and M. Gedvilas, Opt. Express **29**, 7641 (2021).
14. D. Metzner, P. Lickschat, and S. Weißmantel, J. Laser Appl. **33**, 012057 (2021).
15. P. Lickschat, D. Metzner, and S. Weißmantel, J. Laser Appl. **33**, 042002 (2021).
16. D. Metzner, M. Olbrich, P. Lickschat, A. Horn, and S. Weissmantel, J. Laser Appl. **33**, 032014 (2021).
17. S. Liu, B. Zhang, Y. Bu, D. Zhao, X. Zhu, L. Yang, and J. Hou, High Power Laser Sci. Eng. **11**, e81 (2023).
18. H. Kalaycioglu, K. Eken, and F. O. Ilday, Opt. Lett. **36**, 3383 (2011).
19. H. Kalaycioglu, Y. B. Eldeniz, O. Akcaalan, S. Yavas, K. Gurel, M. Efe, and F. O. Ilday, Opt. Lett. **37**, 2586 (2012).
20. H. Kalaycıoğlu, O. Akcaalan, S. Yavas, Y. B. Eldeniz, and F. O. Ilday, J. Opt. Soc. Am. B **32**, 900 (2015).
21. C. Kerse, H. Kalaycioglu, P. Elahi, O. Akcaalan, and F. O. Ilday, Opt. Commun. **366**, 404 (2016).
22. J. M. Liu, X. L. Li, S. M. Zhang, M. M. Han, H. Y. Han, and Z. J. Yang, IEEE J. Sel. Top. Quantum Electron. **25**, 8900106 (2019).
23. T. Bartulevicius, K. Madeikis, L. Veselis, V. Petrauskiene, and A. Michailovas, Opt. Express **28**, 13059 (2020).
24. T. Bartulevicius, M. Lipnickas, V. Petrauskiene, K. Madeikis, and A. Michailovas, Opt. Express **30**, 36849 (2022).
25. G. Sobon, K. Krzempek, P. Kaczmarek, K. M. Abramski, and M. Nikodem, Opt. Commun. **284**, 4203 (2011).
26. C. Lecaplain and P. Grelu, Opt. Express **21**, 10897 (2013).
27. Y. Wang, J. Li, K. Mo, Y. Wang, F. Liu, and Y. Liu, Sci. Rep. **7**, 7779 (2017).
28. A. Martinez and S. Yamashita, Opt. Express **19**, 6155 (2011).
29. R. Thapa, D. Nguyen, J. Zong, and A. Chavez-Pirson, Opt. Lett. **39**, 1418 (2014).
30. Z. Liang, W. Lin, J. Wu, X. Chen, Y. Guo, L. Ling, X. Wei, and Z. Yang, Opt. Lett. **47**, 1867 (2022).
31. Y. Fan, H. Xiu, W. Lin, X. Chen, X. Hu, W. Wang, J. Wen, H. Tian, M. Hao, C. Wei, L. Wang, X. Wei, and Z. Yang, High Power Laser Sci. Eng. **11**, e50 (2023).
32. H. Cheng, W. Lin, Z. Luo, and Z. Yang, IEEE J. Sel. Top. Quantum Electron. **24**, 1100106 (2018).
33. S. Xu, Z. Yang, W. Zhang, X. Wei, Q. Qian, D. Chen, Q. Zhang, S. Shen, M. Peng, and J. Qiu, Opt. Lett. **36**, 3708 (2011).
34. S. H. Xu, Z. M. Yang, T. Liu, W. N. Zhang, Z. M. Feng, Q. Y. Zhang, and Z. H. Jiang, Opt. Express **18**, 1249 (2010).
35. J. Zuo, H. Yu, S. Zou, Z. Dong, C. He, S. Xu, C. Ning, X. Chen, X. Li, and X. Lin, High Power Laser Sci. Eng. **11**, e22 (2023).
36. J. Zuo and X. Lin, Laser Photonics Rev. **16**, 2100741 (2022).
37. H. Yu, J. Y. Zhang, Y. Y. Qi, L. Zhang, S. Z. Zou, L. Wang, and X. C. Lin, J. Lightwave Technol. **33**, 1761 (2015).
38. H. Yu, Y. Y. Qi, J. Y. Zhang, S. Z. Zou, L. Zhang, C. J. He, H. Chen, B. Li, and X. C. Lin, IEEE J. Sel. Top. Quantum Electron. **24**, 3100105 (2018).
39. S. Liu, P. Guo, X. He, Z. Dou, D. Zhao, L. Yang, B. Zhang, and J. Hou, Opt. Express **30**, 4592 (2022).
40. J. Petelin, B. Podobnik, and R. Petkovšek, Appl. Opt. **54**, 4629 (2015).
41. M. Nie, X. Cao, Q. Liu, E. Ji, and X. Fu, Opt. Express **25**, 13557 (2017).
42. X. He, B. Zhang, S. Liu, L. Yang, J. Yao, Q. Wu, Y. Zhao, T. Xun, and J. Hou, High Power Laser Sci. Eng. **9**, e13 (2021).
43. G. Xie, Y. Liu, C. Zhang, Z. Deng, L. Zhou, S. Xiong, Z. Tang, H. Lou, Z. Zhao, D. Luo, C. Gu, and W. Li, Opt. Laser Technol. **151**, 108032 (2022).

https://doi.org/10.1017/hpl.2024.71 Published online by Cambridge University Press

44. D. N. Schimpf, C. Ruchert, D. Nodop, J. Limpert, A. Tünnermann, and F. Salin, Opt. Express **16**, 17637 (2008).
45. A. Malinowski, K. T. Vu, K. K. Chen, J. Nilsson, Y. Jeong, S. Alam, D. Lin, and D. J. Richardson, Opt. Express **17**, 20927 (2009).
46. C. Ning, S. Zou, H. Yu, S. Xu, X. Chen, J. Zuo, S. Han, X. Li, Z. Zhang, C. He, and X. Lin, Opt. Laser Technol. **157**, 108701 (2022).
47. V. Ustimchik, Y. Chamorovskii, and V. Filippov, Proc. SPIE **11981**, 119810T (2022).
48. A. Petrov, M. Odnoblyudov, R. Gumenyuk, L. Minyonok, A. Chumachenko, and V. Filippov, Sci. Rep. **10**, 17781 (2020).
49. X. Ma, C. Zhu, I. N. Hu, A. Kaplan, and A. Galvanauskas, Opt. Express **22**, 9206 (2014).
50. H.-J. Otto, F. Stutzki, N. Modsching, C. Jauregui, J. Limpert, and A. Tünnermann, Opt. Lett. **39**, 6446 (2014).

https://doi.org/10.1017/hpl.2024.71 Published online by Cambridge University Press